Polymer 51 (2010) 3520–3531

Contents lists available at ScienceDirect

Polymer

journal homepage: www.elsevier.com/locate/polymer

Batch foaming of SAN/clay nanocomposites with $scCO_2$: A very tunable way of controlling the cellular morphology

Laetitia Urbanczyk [a], Cédric Calberg [b], Christophe Detrembleur [a], Christine Jérôme [a,*], Michaël Alexandre [a]

[a] Centre for Education and Research on Macromolecules (CERM), University of Liege, Building B6, 4000 Liège, Belgium
[b] Department of Applied Chemistry, University of Liege, Building B6, 4000 Liège, Belgium

ARTICLE INFO

Article history:
Received 23 February 2010
Received in revised form
17 May 2010
Accepted 19 May 2010
Available online 8 June 2010

Keywords:
Foam
CO_2
Clay

ABSTRACT

This paper aims at elucidating some important parameters affecting the cellular morphology of poly (styrene-*co*-acrylonitrile) (SAN)/clay nanocomposite foams prepared with the supercritical CO_2 technology. Prior to foaming experiments, the SAN/CO_2 system has first been studied. The effect of nanoclay on CO_2 sorption/desorption rate into/from SAN is assessed with a gravimetric method. Ideal saturation conditions are then deduced in view of the foaming process. Nanocomposites foaming has first been performed with the one-step foaming process, also called depressurization foaming. Foams with different cellular morphology have been obtained depending on nanoclay dispersion level and foaming conditions. While foaming at low temperature (40 °C) leads to foams with the highest cell density ($\sim 10^{12}$–10^{14} cells/cm^3), the foam expansion is restricted (d ~ 0.7–0.8 g/cm^3). This drawback has been overcome with the use of the two-step foaming process, also called solid-state foaming, where foam expansion occurs during sample dipping in a hot oil bath (d ~ 0.1–0.5 g/cm^3). Different foaming parameters have been varied, and some schemes have been drawn to summarize the characteristics of the foams prepared – cell size, cell density, foam density – depending on both the foaming conditions and nanoclay addition. This result thus illustrates the huge flexibility of the supercritical CO_2 batch foaming process for tuning the foam cellular morphology.

1. Introduction

Conventional polymeric foams are very attractive mostly because of their lower cost per volume unit compared to unfoamed materials, but also for their sound or heat insulating properties, cushioning ability, etc. However, the foams mechanical properties are generally weaker than plain materials, thus limiting their range of applications. Microcellular foams, defined as foams with cell diameter lower than 10 μm and cell density greater than 10^{10} cells/cm^3, usually show better mechanical properties over conventional foams (cell size >300 μm and cell density <10^6 cells/cm^3) [1].

A lot of works and reviews report that supercritical CO_2 is a very efficient foaming agent for microcellular foam processing [1–4]. In addition, CO_2 is environmentally friendly, non toxic, cheap, abundant, and its supercritical parameters are easily attainable (T_c = 31.1 °C, P_c = 73.8 bar). Batch and continuous foaming of polymers with supercritical fluids, and more especially with $scCO_2$, have been extensively described in the literature [4,5]. Basically, the foaming process consists of three main steps. First, the fluid is solubilized into the polymer and the mixture forms a homogeneous phase. Then, a thermodynamic instability is suddenly applied to the system *via* a pressure drop, or a temperature increase, leading to sudden polymer/fluid immiscibility. The system reacts against this perturbation by inducing phase demixion, which usually occurs in the form of cell nucleation. Then, CO_2 molecules migrate towards the nucleated cells and participate to cell growth. Foam expansion occurs until the rising viscosity of the polymer (through cooling, deplasticization, crystallization and/or strain hardening) restricts any additional deformation, or until all the fluid available is used [6,7].

As illustrated in a previous work [8], polymers can be filled with a small amount of nanoparticles, such as lamellar nanoclays, in order to enhance several material properties like reduced flammability and gas permeability, and improved mechanical resistance. Actually, these nanofillers are not only beneficial for material properties, but they are also known to promote the heterogeneous nucleation of extra cells during foaming. Therefore, polymer/clay nanocomposite foams are usually characterized by small cell size and high cell density, which is highly desirable to achieve better mechanical resistance [4]. A lot of works dealing with $scCO_2$-assisted foaming of several nanocomposites systems have already

* Corresponding author. Tel.: +32 43663491; fax: +32 43663497.
E-mail address: c.jerome@ulg.ac.be (C. Jérôme).

0032-3861/$ – see front matter © 2010 Elsevier Ltd. All rights reserved.
doi:10.1016/j.polymer.2010.05.037

been described in the literature, such as blends of polypropylene/clay [9,10], polycarbonate/clay [11], polystyrene/clay [12], polylactide/clay [13–15], polycarbonate/nano-silica [16], polystyrene/carbon nanofibers [17] or polypropylene/nano-$CaCO_3$ [18]. The group of Tomasko, among others, demonstrated the high impact of filler delamination level inside the polymer matrix on polymer foamability as well as on the final foam properties [19]. In fact, they observed a higher cell nucleation efficiency for the exfoliated nanoclays compared to the intercalated ones into PS and PMMA. Indeed, the effective particle concentration is higher in the exfoliated nanocomposites, leading to more efficient heterogeneous nucleation. It must be mentioned that clay treatment also affects its nucleation efficiency by modifying the surface chemistry of the nanofiller, as demonstrated by Zeng et al. [4,19].

In this paper, we focus on the preparation of poly(styrene-*co*-acrylonitrile) foams filled with lamellar nanoclays using $scCO_2$ as a physical blowing agent. The added nanofiller is expected to promote the nucleation of a high number of small cells. Two types of nanoclays with different surface treatments have been selected, *i.e.* Cloisite® 30B and MB30B, a home-made masterbatch prepared in $scCO_2$ based on poly(ε-caprolactone) chains grafted at the surface of Cloisite® 30B platelets (see refs. [8,20]), in order to prepare intercalated and highly exfoliated SAN/clay nanocomposite foams, respectively.

Only a few papers have been found in the literature regarding the production of SAN foams with supercritical carbon dioxide [21,22] or supercritical N_2 [23]. In their paper, Lee et al. [21] studied one-step batch foaming of SAN (*i.e.* foaming occurred during the depressurization step) and investigated the effect of several foaming parameters on foam morphology. In the present study, both SAN and SAN/clay nanocomposites are foamed under two different batch foaming processes. The first one, called the "depressurization (or one-step) foaming process", consists in first saturating the sample with $scCO_2$ in a pressurized vessel at a temperature higher than the T_g of the plasticized polymer. Foaming is then induced by depressurization. The second one is known as the "solid-state (or two-step) foaming process". After CO_2 saturation, the sample is first "frozen" at a temperature below the polymer/CO_2 T_g, then the vessel is depressurized, and foaming is induced by dipping the saturated sample in a hot oil bath (above T_g of plasticized polymer).

According to the scientific literature, the authors use as often the first as the second method, but they systematically focus on a single method. In this work, we use both of them, in order to compare their impact on the foams characteristics. The purpose of this work is thus to investigate the influence of the foaming method, foaming conditions, and nanofillers addition on SAN foam morphology and expansion ratio. Particular attention is paid to the nucleating efficiency of nanoclays depending on their delamination degree as well as on the experimental foaming conditions.

2. Experimental part

2.1. Nanocomposites preparation

Poly(styrene-*co*-acrylonitrile) (SAN) with an AN content of 25 wt% was provided by BASF (Luran®358 N). The montmorillonite clay used, selected from Southern Clay Products (Texas, USA), is organo-modified with bis-(2-(hydroxyethyl)methyl) (tallowalkyl) ammonium cations (Cloisite®30B or C30B). A home-made pre-exfoliated nanoclay masterbatch, MB30B, was also used. MB30B is made of commercial Cloisite®30B treated with ε-caprolactone and tin octoate (II) in $scCO_2$. The details about masterbatch preparation and characterization have been reported in a previous paper [20]. MB30B contains 53 wt% in inorganics and 34 wt% of polycaprolactone (PCL), partially grafted onto the clay surface (Mn ~1500 g/mol, PDI = 1.8). Nanofillers dispersion (C30B or MB30B) into SAN has been performed by melt blending at 175 °C for 5 min in a counter rotating twin-screw internal mixer (Brabender®). The inorganic content was set at 3 wt%. The preparation and characterization of these nanocomposites have been fully described in a former work [8]. The samples have then been molded into 3 mm-thick cylinders with a diameter of 25 mm in a hot press (175 °C) for 5 min. These cylindrical specimens have been used for foaming experiments. Smaller cylinders have been prepared for CO_2 sorption measurements (15 × 1.2 mm).

2.2. Analysis of CO_2/polymer system

CO_2 sorption/desorption experiments have been performed using an *ex situ* gravimetric method called mass-loss analysis, with carbon dioxide obtained from Air Liquide Belgium (purity 99.95%). The technique consists in first treating the cylindrical sample (diameter 15 mm, thickness:1.2 mm) with CO_2 at selected pressure and temperature for a determined sorption time. Then, the pressure is released and the saturated sample is quickly weighted with a high precision balance (Mettler Toledo, precision:0.0001 g) at room temperature. The evolution of the sample weight is followed over time at room temperature. Sample transfer is performed as fast as possible (~45 s after depressurization) in order to limit CO_2 diffusion out of the sample during its handling.

2.3. Foam processing

SAN foams have been prepared according to depressurization foaming (one-step) or solid-state foaming (two-step) processes. For the first method (Fig. 1a), the samples are saturated with CO_2 at 300 bar and 100 °C for 22 h. Then, foaming occurs during vessel depressurization. Fast and slow depressurization times are investigated, and various saturation and foaming temperatures are assessed as well (100, 80, 60 and 40 °C).

For the second method (Fig. 1b), the samples are also saturated at high pressure (300 bar) during 22 h or 48 h (time sufficient to reach equilibrium), but only at low temperature (40 °C). After a determined period of time, the high pressure reactor is cooled to 0 °C before being quickly depressurized (within 3 s), and the sample is then readily removed from the vessel. Cooling the saturated sample is performed for the purpose of restricting/limiting its expansion during depressurization. In the next step, foam expansion is induced by dipping the saturated sample in hot oil bath at 100 °C for a determined period of time, going from 15 s to 5 min. Finally, the foam structure is stabilized by freezing the sample in an ice/water bath.

2.4. Foam characterization

Foam density (ρ_f) is estimated by weighing a foamed sample of known volume, while foam porosity is observed by scanning electron microscopy (SEM; JEOL JSM 840-A) after metallization with Pt (30 nm). Image analysis is manually performed on the basis of SEM pictures by measuring the size of at least 100 cells. Cell density (N_{cell}) relative to unfoamed polymer is estimated according to the following formula [16]:

$$N_{cell} = \left(\frac{n\,M^2}{A}\right)^{3/2} \cdot \frac{\rho_s}{\rho_f} \quad (1)$$

where n is the number of cells in the SEM picture, M the magnification, A the surface area of the picture (cm^2) and ρ_s and ρ_f are respectively the solid and foamed sample densities.

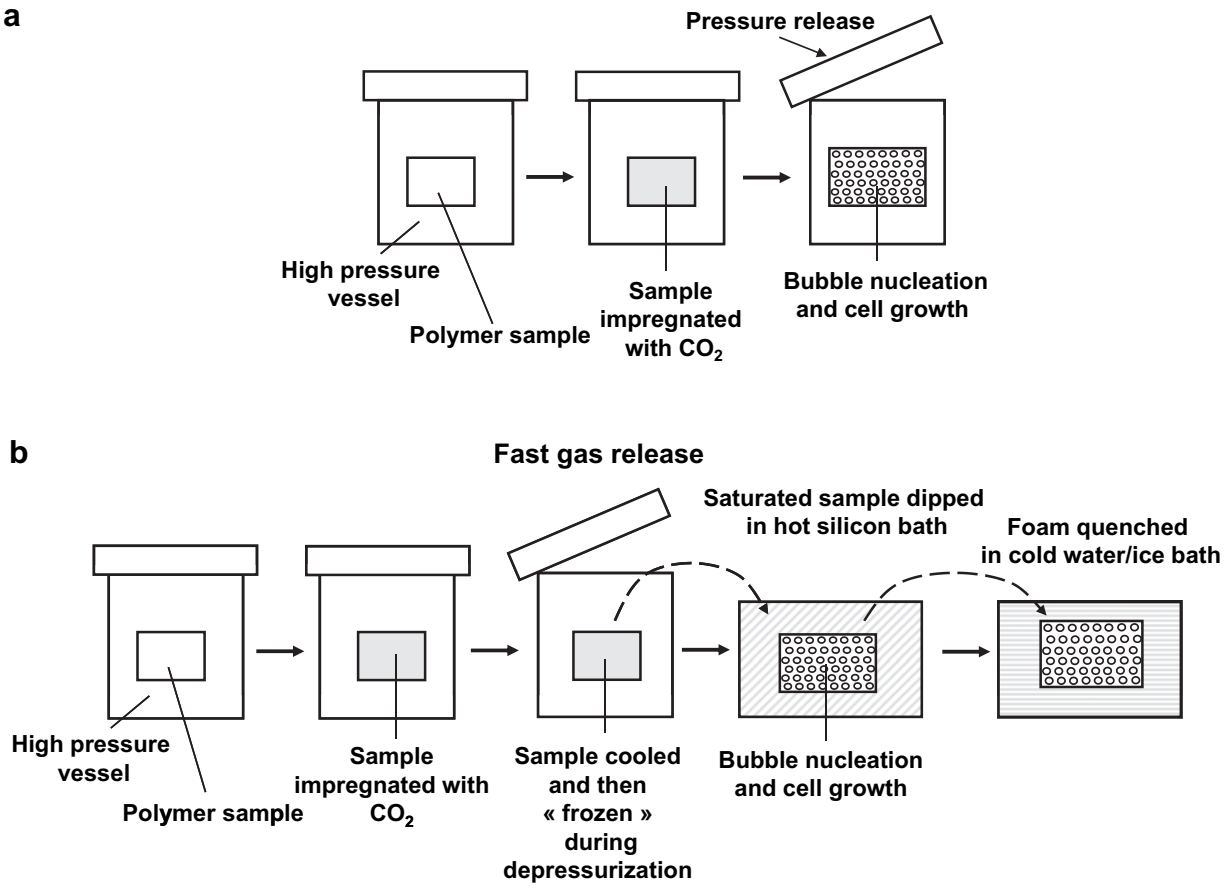

Fig. 1. Illustration of a) depressurization foaming method (one-step), and b) solid-state foaming method (two-step) used to prepare polymeric foams.

3. Results and discussion

3.1. Nanocomposites morphology

The characteristics of two kinds of nanocomposites prepared in a previous work [8] are summarized in Table 1, where SAN/C30B is an intercalated nanocomposite while the clay in SAN/MB30B is mainly exfoliated. These two samples have been selected for the foaming process for the purpose of examining the impact of nanoclay dispersion level on foam morphology.

3.2. CO_2 solubility and diffusivity in SAN

CO_2 diffusivity into and from SAN has been studied with the purpose of determining accurate saturation conditions in view of the foaming process. CO_2 solubility values were extracted from CO_2 desorption curves and related to saturation conditions. Whether nanoclay influences CO_2 sorption/desorption rates was assessed as well.

Table 1
Characteristics of the nanocomposites to be foamed (filled with 3 wt% in inorganics).

Sample	Nanoclay type	Interlayer distance (nm)[a]	Visual aspect	Nanocomposite morphology[b]
SAN	none	–	Translucent	–
SAN/C30B	Cloisite® 30B	3.5	Cloudy with visible clay stacks	Mainly intercalated
SAN/MB30B	Masterbatch MB30B	Very weak signal	Translucent, no clay stack	Mainly exfoliated

[a] Determined by X-ray analysis.
[b] Deduced from X-ray and TEM analyses, as well as visual aspect.

Some very accurate techniques allow an *in situ* determination of CO_2 diffusivity/sorption into polymers, like 1) the pressure decay method (also called PVT method), which follows the change of pressure or volume during saturation of a polymer sample of known volume [24], or 2) the *in situ* gravimetric method, which consists in measuring the weight uptake of the sample *in situ* during fluid sorption with an electronic microbalance or magnetic suspension balance [25]. The first technique requires very precise calibration, while the second is usually limited to low CO_2 pressure (<60 bar). When none of these specific apparatuses are available, an *ex situ* gravimetric method can also be applied by weighting the saturated sample right after depressurization and removal from the reactor with a high precision balance at room pressure and temperature. This mass-loss analysis technique is used in the present study. However, fluid escape from the sample is unavoidable during its transfer from the vessel to the balance, and this will undoubtedly lead to an underestimation of the amount of CO_2 sorbed under the selected saturation conditions. In order to limit this error, CO_2 desorption rate can be followed *via* the evolution of the sample weight in function of time. The weight percentage of CO_2 sorbed at time t ($M_{gas,t}$) can be calculated from the sample weight at time t (M_t) and the initial sample weight (M_i, before the experiment), according to the formula: $M_{gas,t} = (M_t - M_i)/M_i \times 100$. The initial amount of CO_2 sorbed at $t = 0$ ($M_{gas,0}$), *i.e.* right after depressurization, can be roughly estimated by extrapolating the plot of $M_{gas,t}$ against time at $t = 0$. This technique is illustrated in

Fig. 2, with a typical graph corresponding to CO_2 desorption from SAN sample in function of time. The dotted curve represents the extrapolation towards $t = 0$, allowing the determination of $M_{gas,0}$. However, this kind of extrapolation is subjective and rather leads to a rough approximation of the initial amount of fluid solubilized.

In order to enhance the accuracy of $M_{gas,0}$ determination, the desorption curve can be plotted in function of the square root of desorption time (Fig. 3). If the initial part of the curve follows a linear trend, Fickian diffusion can be assumed [26], *i.e.* the desorption diffusion coefficient, D_d, is time independent. Then, the initial part of the curve can be approximated with Equation (2) [27], which relies on the following assumptions: 1) the diffusion coefficient is fluid concentration independent, 2) fluid concentration is uniform throughout the sample, and 3) diffusion occurs exclusively in one direction, *i.e.* perpendicular to sample surface (flat plate):

$$\frac{M_{d,t}}{M_{gas,0}} = \frac{4}{l}\cdot\sqrt{\frac{D_d \cdot t_d}{\pi}} \tag{2}$$

where l is the sample thickness, and $M_{d,t}$ is the weight desorbed at time t, and equals $M_{gas,0} - M_{gas,t}$. This Equation can be re-written

$$1 - \frac{M_{d,t}}{M_{gas,0}} = 1 - \frac{4}{l}\cdot\sqrt{\frac{D_d \cdot t_d}{\pi}} \text{ or}$$

$$M_{gas,t} = M_{gas,0} - \frac{4}{l}\cdot\sqrt{\frac{D_d \cdot t_d}{\pi}}\cdot M_{gas,0} \tag{3}$$

Thus, the plot of $M_{gas,t}$ against $t_d^{1/2}$ (Fig. 3) at short $t_d^{1/2}$ values gives access to both $M_{gas,0}$ (intercept at $t = 0$) and D_d (proportional to the slope of the curve). The desorption curves corresponding to SAN and SAN/clay composites at different sorption times are presented in Fig. 3. D_d values, deduced from these curves and calculated with Equation (3), are plotted in function of the amount of fluid absorbed in Fig. 4.

From this graph, one can observe a progressive increase of D_d with an increase of CO_2 content solubilized at CO_2 content <18 wt%, while a jump of D_d values is clearly observed above 18–20 wt% of CO_2. Carbon dioxide is known to act as a plasticizer when dissolved into many polymers [28,29]. In other words, CO_2 increases the chain mobility and decreases the polymer glass transition temperature (T_g). The more the fluid sorbed, the higher the plasticization and thus, the fastest the fluid desorption from the sample. The D_d jump observed at CO_2 content above 18–20 wt% should result from the expected polymer transition from glassy to rubbery state due to a T_g decrease of the SAN/CO_2 system below room temperature. The cloudy aspect of the specimens treated for at least

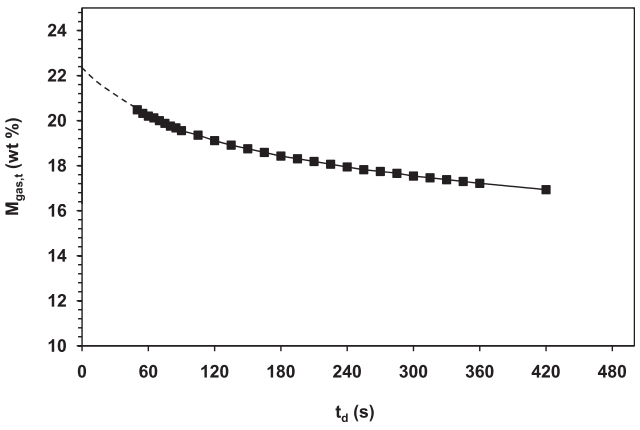

Fig. 2. Desorption curve of SAN sample saturated with CO_2 for 3 h at 40 °C and 300 bar.

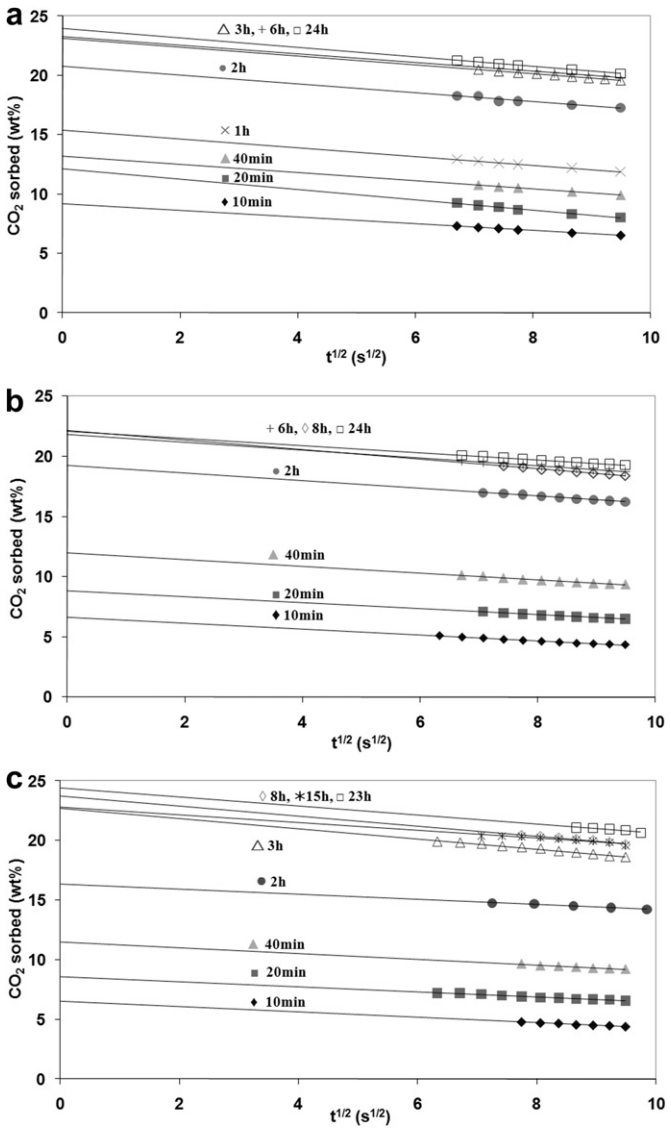

Fig. 3. Plots of the amount of CO_2 sorbed ($M_{gas,t}$) against the square root of desorption time ($t_d^{1/2}$) for short $t_d^{1/2}$. a) SAN, b) SAN/C30B, and c) SAN/MB30B. Specimens are saturated with CO_2 at 40 °C and 300 bar for different sorption times.

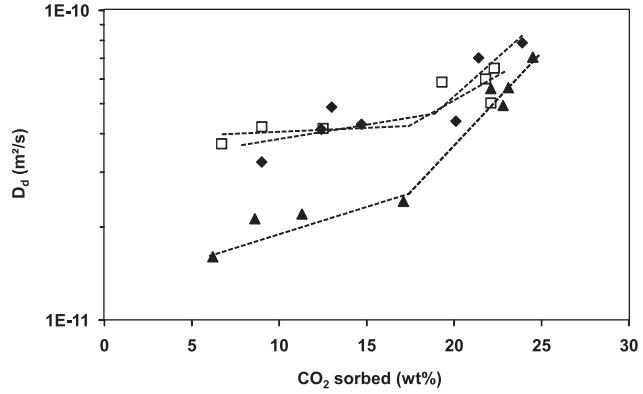

Fig. 4. Influence of the amount of CO_2 sorbed ($M_{gas,0}$) on desorption diffusion coefficient (D_d) of SAN (◆), SAN/C30B (□) and SAN/MB30B (▲) specimens. D_d values are deduced from the slope of desorption curves of Fig. 3. Dotted lines are only guide for the eyes.

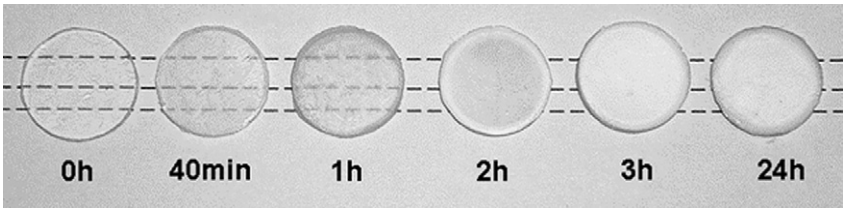

Fig. 5. Photographs of SAN specimens saturated for increasing sorption periods under constant saturation conditions (40 °C, 300 bar).

2 h with CO_2 already attests for decreased T_g below 40 °C (Fig. 5) due to gas demixion in the rubbery-like material. This assumption has been experimentally confirmed with some DSC measurements performed on samples saturated with CO_2 (data not shown). However, there is a huge uncertainty associated with the measurements performed at ambient pressure due to fluid escape during the test [30]. Anyway, the T_g value obtained for the sample saturated for 24 h at 40 °C and 300 bar of CO_2 was well below 0 °C, which confirms SAN plasticization by CO_2.

D_d does not seem to be greatly affected by 3 wt% of intercalated nanoclay added. In contrast, addition of the same amount of exfoliated clay leads to considerable decrease of desorption rate when the sample is in its glassy state (<18 wt% of CO_2 sorbed). The effect is much less pronounced when the plasticized sample is in its rubbery state. This result is in accordance with the observations made by Lee et al. on PS/clay nanocomposites [4].

In the present case, nanoclay dispersion level and the state of the polymer are found to be two important factors affecting the rate of CO_2 desorption. Indeed, nanometric inorganic platelets are non permeable to gases and thus increase the tortuosity, or path length, for CO_2 molecules to cross the sample width. It has been previously shown [8] that exfoliated nanoclay leads to higher decrease of gaseous CO_2 permeability in SAN compared to the intercalated one. This was explained by higher aspect ratio and thus by higher number of effective particles in the matter. This data is thus in accordance with the reduced CO_2 desorption rate observed in the current study. However, when the polymer softens (above T_g), CO_2 diffusivity increases significantly and the effect of nanoclay becomes less pronounced. This different behavior might be explained by different diffusion processes due to cells which may have nucleated during depressurization (phase demixion).

The amount of fluid sorbed, $M_{gas,0}$, determined from desorption curves, has been plotted in function of sorption time, t_s, in Fig. 6. The curves obtained allow for an estimation of the saturation time necessary to reach the equilibrium ($t_{s,eq}$), *i.e.* to solubilize the maximum amount of CO_2 (M_∞) in SAN under the selected conditions. The curve of $M_{gas,0}$ against t_s gradually increases and then levels off when the maximum amount of fluid is solubilized in the sample under the investigated conditions. M_∞ lies around 24 wt% of CO_2 for SAN and SAN/clay nanocomposites at 40 °C and 300 bar, and the nanofiller does not influence notably M_∞. It is amazing to notice that almost 10 wt% of $scCO_2$ can be sorbed in SAN within only 20 min! This demonstrates the exceptional affinity between SAN and CO_2. This high affinity is certainly due to polar interactions between CO_2 and nitrile groups of SAN. For the sake of comparison, we performed a sorption experiment with PS (0 wt% AN, 143E from BASF, M_n = 117,000 g/mol, M_w/M_n = 2.6, 40 °C, 300 bar, 24 h). The amount of CO_2 sorbed by PS under these conditions reached 16 wt %, which is lower than our SAN (24 wt% CO_2, 25 wt% AN). From Fig. 6, it can be estimated that a t_s of minimum 8 h is required to ensure the equilibrium of fluid saturation at 40 °C and 300 bar for 1.2 mm-thick samples.

The initial part of the sorption curve of SAN/MB30B is delayed compared to SAN and SAN/C30B (especially at 2 h sorption time, Fig. 6). This behavior is consistent with lower CO_2 diffusivity rate due to the exfoliated clay. The delay is then compensated at longer t_s thanks to highly increased fluid diffusivity caused by important polymer plasticization above 18 wt% of CO_2.

Finally, the amount of CO_2 sorbed in SAN has been investigated as a function of saturation temperature, again with the desorption technique, while keeping constant pressure (300 bar) and saturation time (24 h). It appears in Fig. 7 that M_∞ decreases with an increase in temperature. This behavior can be attributed to lower fluid density at higher temperature, as shown in Fig. 7 [31].

It is anticipated that $t_{s,eq}$ would decrease when CO_2 saturation occurs at higher temperature, due to higher fluid diffusivity at higher temperature and also to higher polymer chain mobility, especially above T_g. Anyway, foaming experiments performed in the next section on 3 mm-thick samples were conducted for 48 h soaking time (otherwise stated), whatever the saturation temperature, for the sake of comparison. Doing so, we assume complete and homogeneous CO_2 saturation of all samples.

To conclude, with this set of experiments, we have been able 1) to show that exfoliated nanoclay slowed down CO_2 sorption/desorption rate from glassy samples; 2) to determine the minimum saturation time required for 1.2 mm-thick samples to be uniformly saturated with CO_2 at 40 °C and 300 bar; and 3) to estimate the amount of CO_2 sorbed in SAN as a function of saturation temperature.

3.3. Foaming with the depressurization foaming process (one-step)

3.3.1. Effect of depressurization rate

Depressurization foaming is a batch foaming technique which consists in saturating the sample with CO_2 in a high pressure vessel at a temperature above the glass transition temperature of the polymer/CO_2 mixture, and then to depressurize the vessel. Foaming occurs during depressurization as a result of sudden fluid

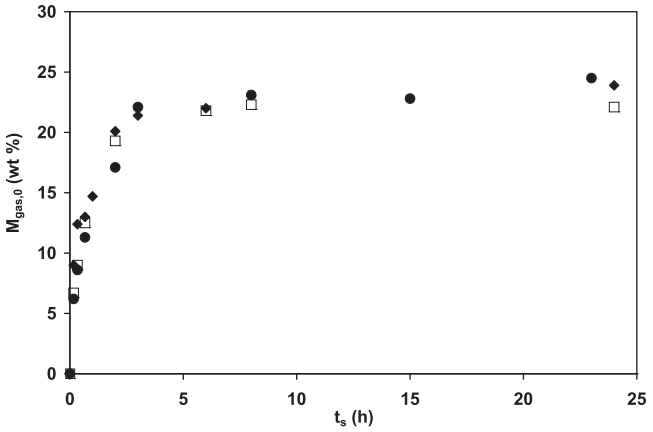

Fig. 6. Sorption curves of SAN (◆), SAN/C30B (□) and SAN/MB30B (●) specimens, saturated with CO_2 at 40 °C and 300 bar, in function of sorption time (t_s). All $M_{gas,0}$ values are deduced from desorption curves (Fig. 4).

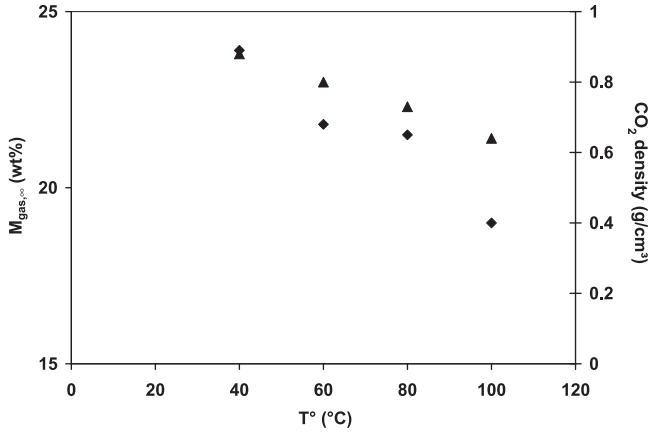

Fig. 7. Equilibrium amount of CO_2 sorbed into SAN at 300 bar for 24 h in function of (◆) saturation temperature and (▲) its correlation with CO_2 density [31].

supersaturation and consequent phase demixion. Fluid demixion usually occurs in the form of cell nucleation. Fig. 1a illustrates this foaming method.

We have first investigated the effects of nanoclay addition and depressurization rate on foam characteristics, such as cell size, cell density and foam density. Micrographs of SAN-based foams produced with a slow depressurization rate (0.5 bar/s on average) are presented in Fig. 8A. Those foams are characterized by densities of 0.2–0.26 g/cm^3 with pore sizes around 10–90 μm for pure SAN and 10–70 μm for nanocomposite foams. Their cell size distribution follows a Gaussian trend. We can observe in Fig. 9 an increase of cell density upon nanofiller addition. In fact, the number of cells nucleated per cm^3 of pure SAN foam (2.2×10^7 cells/cm^3) more than doubles with the addition of 3 wt% of intercalated nanoclay (5.3×10^7 cells/cm^3) and almost triples with the same amount of exfoliated clay (6.2×10^7 cells/cm^3). Thus, we can affirm that nanoclay induces heterogeneous bubble nucleation in SAN under these foaming conditions, and its efficiency is found to be dependent on its delamination degree inside the host polymer.

Faster depressurizing conditions (100 bar/s on average) result in higher foam densities (0.41–0.46 g/cm^3) due to the rapid freezing of the sample under sharp depressurization (fast temperature drop due to Joule-Thompson effect). The foams are characterized by cells of about 1–5 μm in diameter (Fig. 8B) and cell densities around 10^{10} cells/cm^3. Such an increase in cell density compared to foams prepared by slow pressure release rate is related to the higher thermodynamic instability resulting from sharper pressure drop [32–34]. Thus, more carbon dioxide is used for cell nucleation instead of cell growth. Therefore, the cells are accordingly smaller than at slow depressurization rate. Here, the intercalated clay slightly decreases the cell density of SAN foam from 6.5×10^{10} cells/cm^3 to 5.1×10^{10} cells/cm^3, while the exfoliated nanocomposite foam shows a slight increase of the cell density to reach 8×10^{10} cells/cm^3 (Fig. 9). Actually, these fluctuations seem irrelevant when considering the error bars associated with average cell density values.

Some other works also report on the nucleating ability of lamellar nanoclays during foaming with supercritical CO_2. However, the impact of the nanofiller on the number of nucleated cells is usually stronger, and cell density jumps from one to two orders of magnitude are often reported for nanocomposite foams prepared by extrusion foaming [35,36] or foamed in batch [9,11,37–39]. This difference may be explained by the foaming conditions used (see below).

3.3.2. *Effect of saturation/foaming temperature*

It has been demonstrated in the beginning of this paper that decreasing the saturation temperature leads to an increase of CO_2 content sorbed in the polymer. Under high CO_2 concentration, the glass transition temperature of SAN is also highly decreased. In the mean time, foam expansion of samples saturated at lower saturation temperature with the one-step process will occur at lower temperature too. In that context, it is interesting to investigate the overall effect of saturation/foaming temperature on foam expansion ratio and cellular morphology.

Fig. 10 shows SEM pictures of the foams produced by saturation and fast depressurization foaming at a) 100 °C, b) 80 °C, c) 60 °C, and d) 40 °C, while Fig. 11 illustrates the evolution of cell density and foam density with temperature and nanoclay addition.

From SEM pictures, it appears clearly that cell size greatly decreases with a decrease of the saturation/foaming temperature. Indeed, the average pore diameter of pure SAN foam evolves from 5 μm at 100 °C (a-1) to around 1 μm at 40 °C (d-1). The effect of nanoclay on cell size becomes discernible on the micrography at

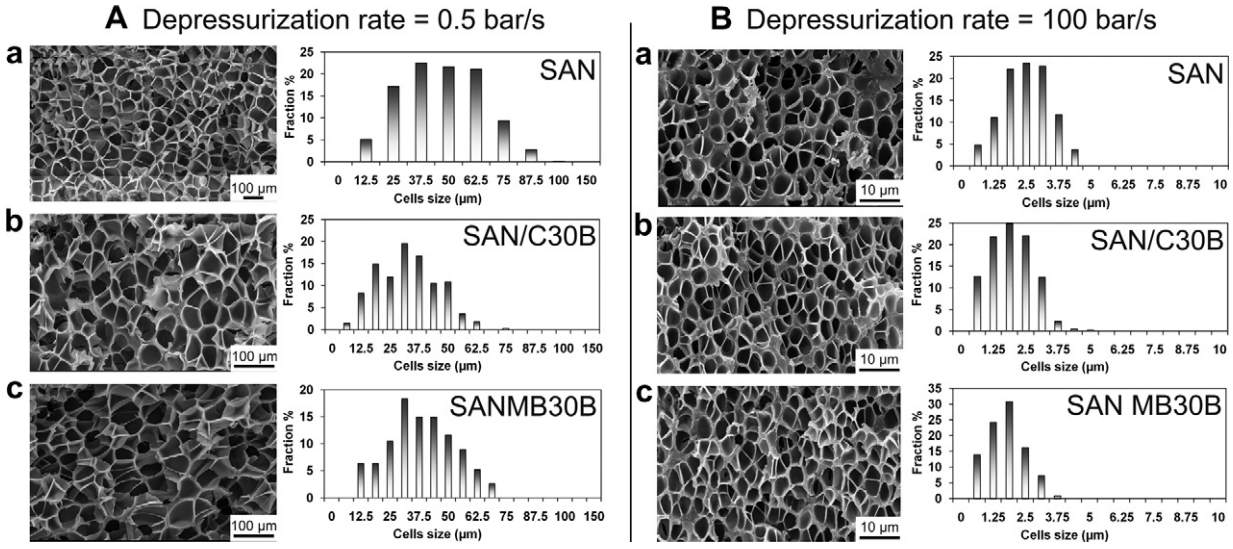

Fig. 8. SEM micrographs and corresponding cell size distribution of SAN-based foams prepared with the one-step foaming process. Samples are saturated with CO_2 at 100 °C, 300 bar for 48 h. Foaming is induced with A) slow depressurization rate (Magnification: 200×) or B) fast depressurization rate (Magnification: 2000×). a) Pure SAN foam, b) SAN/C30B foam and c) SAN/MB30B foam.

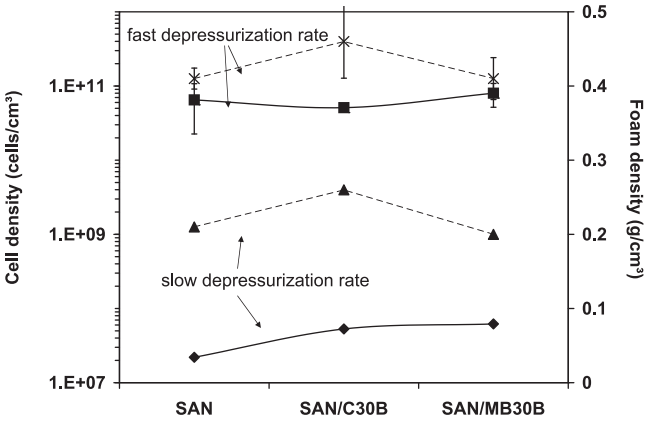

Fig. 9. Evolution of cell density (plain lines) and foam density (dashed lines) of SAN-based foams with nanoclay addition and CO_2 depressurization rate. The samples are saturated at 100 °C and 300 bar for 48 h. Foams prepared with fast depressurization have been performed twice, and average values are reported with the corresponding error bars.

60 °C (c-2, c-3) and is obvious at 40 °C (d-2, d-3), with a clear drop of cell size below the micrometer range.

Foam density is clearly affected by the saturation temperature as shown by the trend of the dashed curves in Fig. 11. In fact, the foam density increases from 0.4 to 0.8 g/cm^3 with a decrease of saturation/foaming temperature from 100 to 40 °C. The expansion ratio is thus restricted at lower saturation/foaming temperature. Indeed, fast viscosity jump occurs during depressurization due to quick sample freezing below T_g. The intercalated clay seems to slightly restrict foam expansion whereas exfoliated nanoclay leads to more expanded foams, at least when foaming occurs at 40 or 60 °C. The clay thus influences foam expansion ratio in a complex way. On one side, clay is known to increase the polymer viscosity, and this may restrict foam expansion. On the other side, we have shown that the lamellar filler can slow down CO_2 desorption rate from the polymer, especially the exfoliated clay. This property could contribute to higher expansion ratio thanks to the extra fluid retained inside the sample, which can take part to cell growth step. Otherwise, this portion of fluid would have quickly diffused out of the sample without contributing to foam expansion due to its very high diffusivity. This is the combination of these effects which is believed to dictate the overall impact of nanoclay on the foam expansion ratio. In the case of SAN/C30B, viscosity effect seems to get the upper hand over fluid trapping, while this balance is reversed for SAN/MB30B composite. This result is in accordance with the finding that exfoliated clay exhibits better gas barrier properties compared to intercalated clay.

The number of cells nucleated in pure SAN foam increases with decreasing foaming temperature, from 6.5×10^{10} cells/cm^3 (100 °C) to 5.35×10^{11} cells/cm^3 (40 °C). This can be attributed to the increasing amount of CO_2 sorbed (*cf* Fig. 7 in Section 3.2), which increases the rate of cell nucleation. Thus, at low temperature, more CO_2 is used for cell nucleation, and less fluid is available for the cell growth step. As discussed in the previous section, the added nanoclay has only a slight influence on SAN foams cell density at

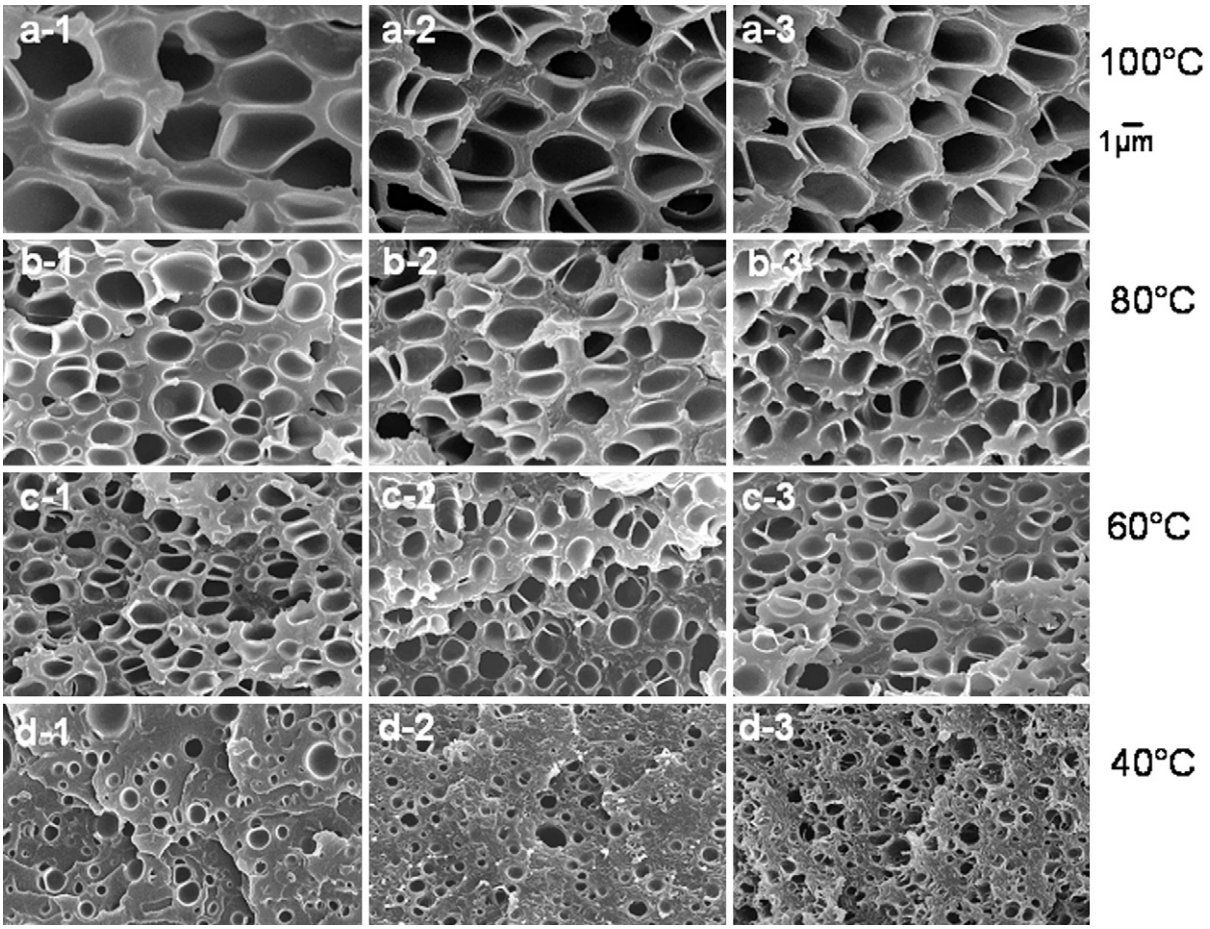

Fig. 10. SEM pictures of 1) SAN, 2) SAN/C30B and 3) SAN/MB30B foams prepared by depressurization foaming at 300 bar of CO_2 and saturation/foaming temperature of a) 100 °C, b) 80 °C, c) 60 °C and d) 40 °C.

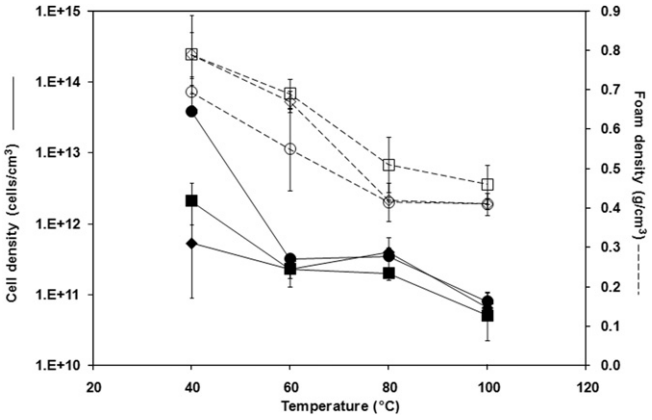

Fig. 11. Cell density (plain lines, filled symbols) and foam density (dashed lines, empty symbols) of SAN (◆), SAN/C30B (■), SAN/MB30B (●) in function of saturation/foaming temperature (one-step foaming process, fast depressurization rate). Experiments have been performed twice and the average cell density and foam density values are presented.

100 °C. It is very interesting to see that its influence becomes suddenly drastic at 40 °C (Fig. 11). Also, it appears that exfoliated nanoclay (4×10^{13} cells/cm^3) is a much more efficient heterogeneous nucleating agent than intercalated nanoclay (2.1×10^{12} cells/cm^3) at this low temperature (pure SAN, 5×10^{11} cells/cm^3). This important result shows that the nucleation ability of nanoclay depends not only on its delamination degree, but also on the foaming conditions. Indeed, at 100 °C, the cell density of pure SAN foam is only nearly doubled with 3 wt% of exfoliated clay (MB30B), while at 40 °C, cell density of pure SAN foam jumps by two orders of magnitude due to the same exfoliated nanoclay! This phenomenon could be partly explained by the higher CO_2 concentration participating to cell nucleation at lower temperature in the nanocomposite, which results from reduced CO_2 desorption rate (Fig. 4). However, CO_2 loss must be minimal under one-step foaming method and thus, this explanation alone cannot support the experimental observations.

In the literature, very few studies mention the effect of foaming conditions when dealing with the heterogeneous nucleating ability of fillers in batch-prepared foams. They rather focus on the amount of nanofiller added or their nature and keep constant foaming conditions [35]. However, the results of this study show that the nucleating efficiency of nanoclays is found to be highly dependent on the foaming conditions. In this context, a review by Gendron et al. [39] discuss the evolution of cell density of PLA and PP foams filled with talc prepared by extrusion foaming in function of CO_2 content. At low CO_2 loading, talc was found to substantially increase the cell density compared to neat foam, while its effect disappeared above a critical CO_2 level (4.5 wt% for PP and 7 wt% for PLA). Of course, the systems mentioned from the literature are very different from the one presented in this work, because in the cited works, foaming occurs continuously in an extruder, while batch foaming is used in the present study. Anyway, an analogy can be found between both systems, because either at low CO_2 content (continuous process) or at low temperature (batch process), the viscosity of the system is higher than at higher CO_2 content/higher temperature. It is believed that system with higher viscosity would be more favorable to heterogeneous cell nucleation. This thought comes both from the observations made in this study and from several works dealing with the understanding of cell nucleation mechanism. In that context, shear-induced nucleation is a very interesting notion to introduce. In a few words, some extra cells have been observed to nucleate when some stress was applied to polymer/CO_2 systems, like mechanical vibrations [40,41], ultrasonic vibrations [42] or shear stress close to the wall of an extruder die [43]. In fact, Zhang et al. [40] showed that applying some vibrations during melt mixing increased the melt strength, and that higher melt strength favored higher cell densities, due to better cell stabilization [44]. Zhu et al. [41] referred to enhanced nucleation driving force to explain increased cell density induced by mechanical vibration. These examples attest that melt viscosity and shear stress are two linked parameters which affect greatly cell density. In the present study, neither vibration nor flow-induced shear stress is applied, because foaming is performed under static conditions. However, nanoclay addition is known to increase the melt viscosity. In a pioneering work, Okamoto showed that isolated platelets close to the wall of an expanding cell tend to orient themselves along the elongational flow during cell expansion [45]. High melt viscosity is believed to trigger high stress at/near the platelets edges during orientation [35]. Some extra cells might originate from this local stress and this would explain higher cell densities observed. Actually, these assumptions have not been proved and would require deeper investigation in order to better understand the heterogeneous nucleation mechanism.

To conclude, this set of experiments allows us to evidence the foaming conditions leading to very high cell densities, *i.e.* low temperature and high pressure. However, decreasing the foaming temperature not only increases the cell density, but also restricts the foam expansion. The next section describes an alternative batch foaming method which aims at better controlling the expansion ratio of high cell density foams.

3.4. Foaming with the solid-state foaming process (two-step)

In the solid-state foaming process, the polymer is saturated with CO_2 at 300 bar and at low temperature (40 °C). After 22 h or 48 h (time sufficient to reach equilibrium), the reactor is cooled at 0 °C before depressurization in order to freeze the polymer and prevent/limit its foaming. Foam expansion is then induced by dipping the saturated sample in a 100 °C oil bath during a few seconds to a few minutes. Finally, the foam structure is stabilized in a water/ice bath (Fig. 1b). The huge advantage of this two-step process is that the foaming conditions can be controlled independently from the CO_2 sorption step.

Pure SAN foams were first prepared with the solid-state foaming process and the effect of the foaming time on the foam morphology was investigated. An increase of the foaming time (*i.e.* the dipping time in the hot bath) from 15 s to 5 min, while keeping the other conditions constant, results in an increase of cell size from 1 to several microns together with a decrease of the foam density from 0.57 to 0.11 g/cm^3 (Figs. 12 and 13).

This is consistent with the increased time allowed for foam expansion. Cell size distribution is narrow for all the investigated foaming times. The samples dipped in the bath for 3 and 5 min are quite similar. This means that maximum foam expansion has been reached within 3 min of foaming under these conditions. Cell density increases with the foaming time, from 5.5×10^{11} cells/cm^3 for 15 sec foaming up to 1.5×10^{12} cells/cm^3 after 5 min. Even if cell nucleation is supposed to occur at the very beginning of the dipping step during a short period of time [10], some cells clearly still nucleate during cell growth.

Fig. 14 shows the morphology of neat and nanocomposite foams obtained after saturation at 40 °C for 48 h and foaming for 3 min at 100 °C, while characteristics of the foams prepared with both foaming processes (one-step and two-step) are compared in Fig. 15. As can be seen in Fig. 14, the cell size distribution narrows upon nanoclay addition and cell size is significantly decreased. The

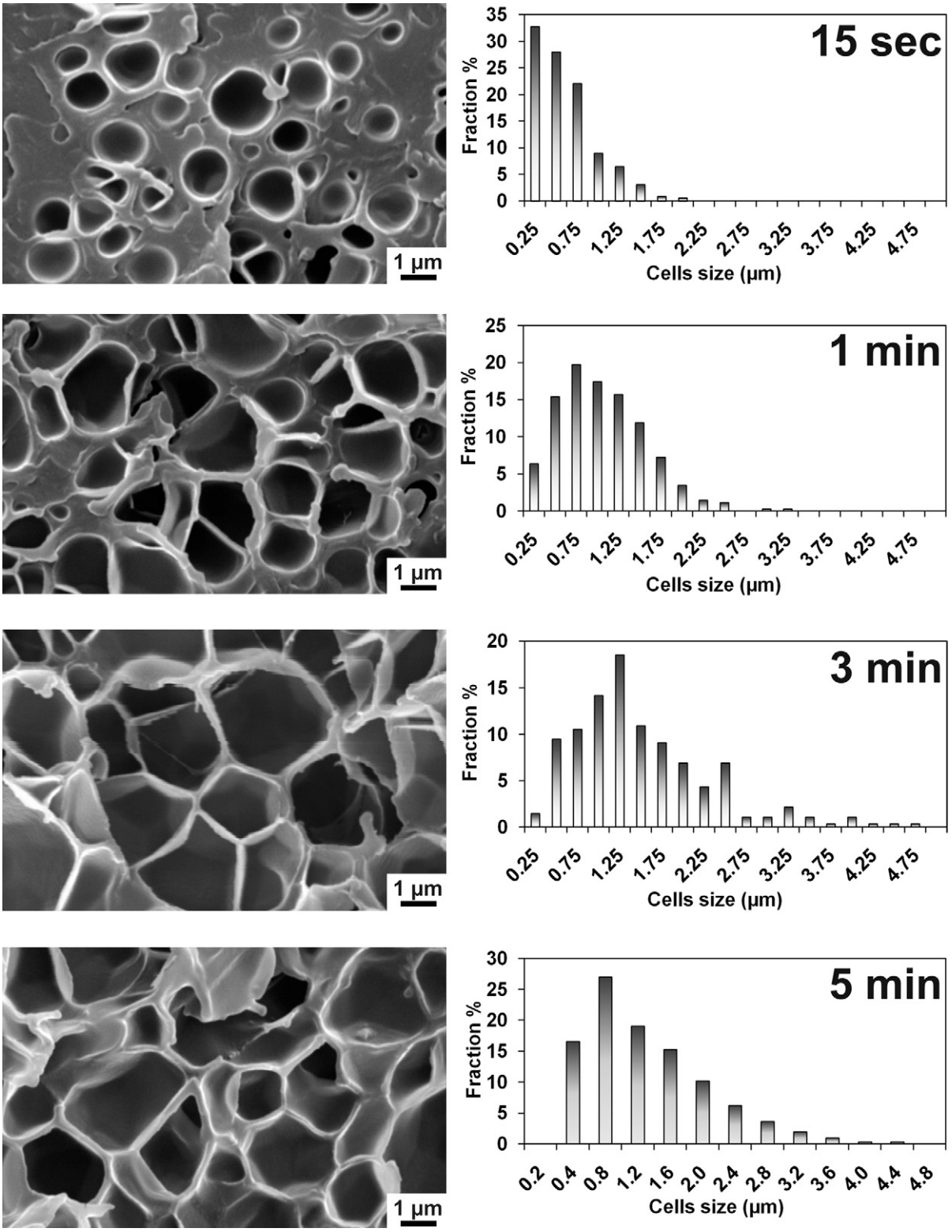

Fig. 12. Cell size distribution and SEM images of pure SAN foams prepared with the solid-state foaming process at different foaming times. The samples are saturated at 40 °C, 300 bar of CO_2 for 22 h and foamed in a 100 °C bath.

nanofiller added also increases significantly the average cell density, from 8.5×10^{11} cells/cm^3 for pure SAN foam, to 3.6×10^{12} cells/cm^3 for the intercalated nanocomposite and 7.6×10^{13} cells/cm^3 for SAN containing the exfoliated clay. Thus, the clay clearly acts as an effective heterogeneous nucleating agent, its efficiency being dependent on its dispersion state. These observations are similar to those previously found for similar foams prepared by depressurization foaming. Nevertheless, the amount of cells nucleated with this solid-state foaming method (8.5×10^{11} cells/cm^3) was found to be slightly higher than with the one-step

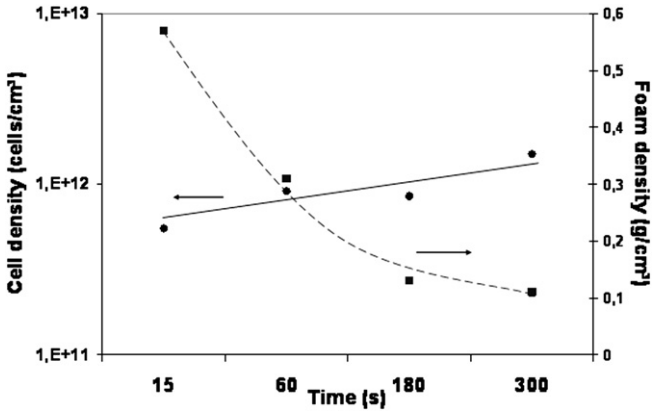

Fig. 13. Evolution of the cell density (●, plain line) and foam density (■, dashed line) of SAN foams as a function of the foaming time. The foams are prepared with the two-step foaming process: saturation at 40 °C and 300 bar of CO_2 for 22 h, foaming in a 100 °C bath.

foaming process (5.3×10^{11} cells/cm^3), despite the fact that samples were saturated under exactly the same conditions (same carbon dioxide content sorbed). This difference may be related to the fact that in the two-step foaming process, the sample is cooled prior to depressurization. The cooled sample should thus exhibit higher melt strength, which would promote higher cell density [44].

Fig. 15 shows that foam density is significantly decreased with the two-step foaming process. In fact, while foam expansion was restricted with the first foaming method, the second one permits a very good control of the time allowed for foam expansion. With the solid-state foaming process, it becomes possible to prepare highly expanded foams (0.12 g/cm^3) characterized by high cell density ($>10^{12}$ cells/cm^3). Nevertheless, foam expansion is still restricted for SAN/MB30B sample (0.53 g/cm^3), whatever the foaming time. This surprising result might be related to higher polymer viscosity associated with the introduction of highly exfoliated nanoclay.

In light of these experiments, two schemes have been drawn for the purpose of illustrating the high flexibility of supercritical CO_2

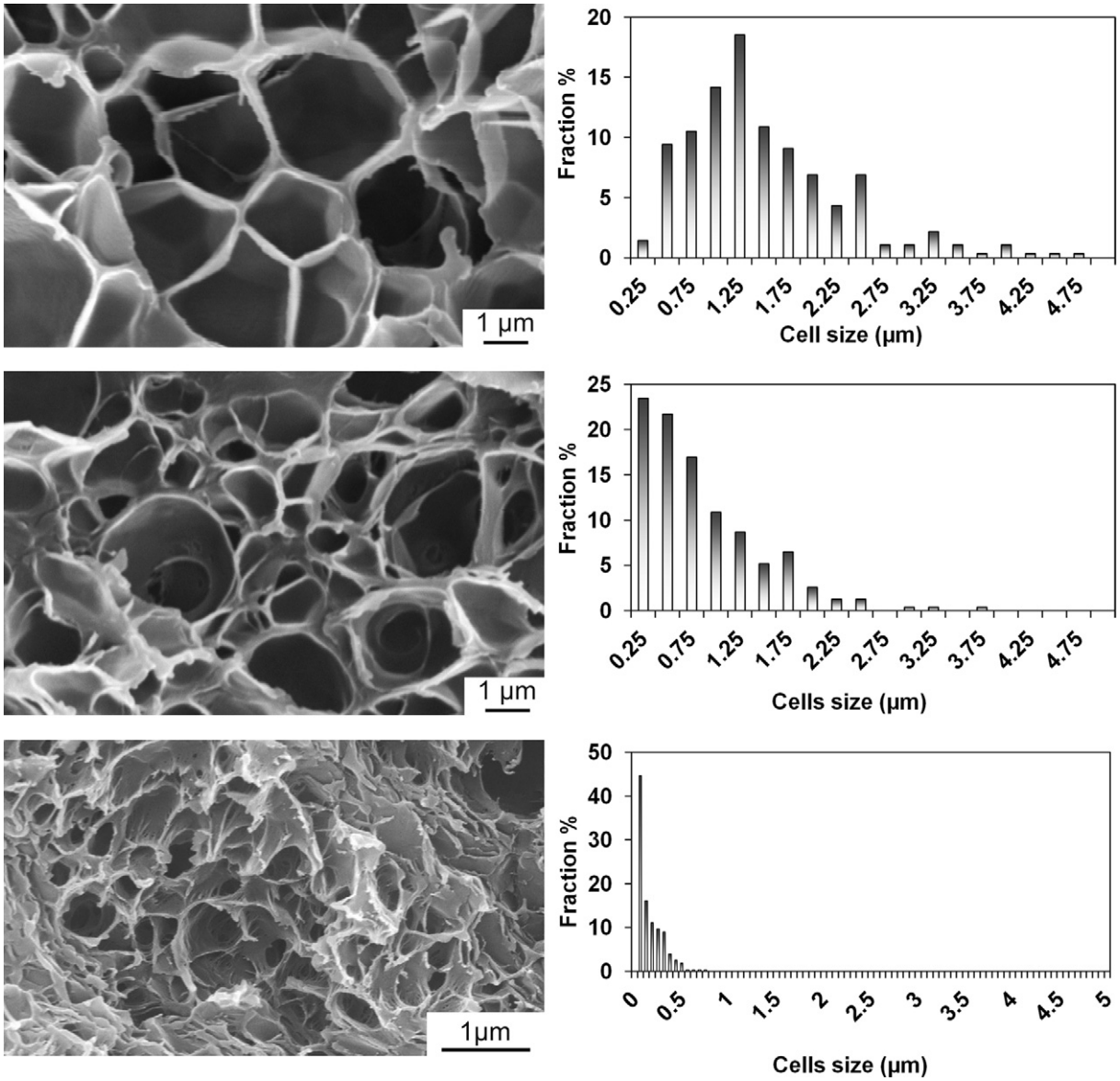

Fig. 14. Effect of nanoclay on morphology and cell size distribution of a) SAN foam, b) SAN/C30B foam, and c) SAN/MB30B foam, saturated with CO_2 at 40 °C, 300 bar, 48 h, and foamed for 3 min at 100 °C (two-step foaming process).

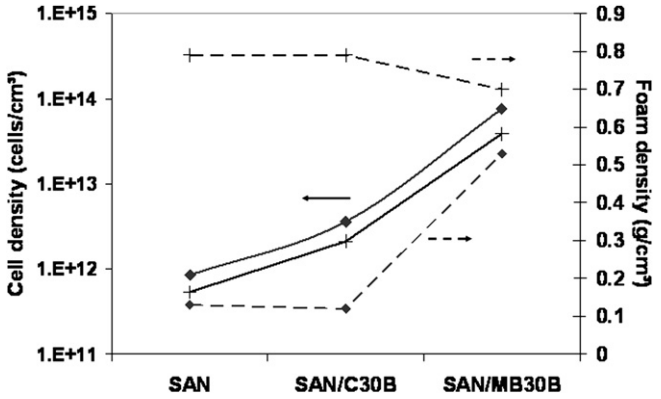

Fig. 15. Evolution of the cell density (plain lines) and foam density (dashed lines) of SAN foamed with the one-step (+) and two-step (◆) foaming processes in function of nanoclay addition. The samples are saturated for 48 h at 40 °C and 300 bar in both cases.

foaming process in producing SAN-based foams with a large panel of morphologies (Fig. 16).

In fact, by varying several foaming conditions, we managed to prepare SAN foams with cell sizes ranging from 1 to 75 μm, cell densities from 10^7 to 10^{12} cells/cm^3, and expansion ratios from 8.3 to 1.4 (*i.e.* foam densities from 0.12 to 0.7 g/cm^3). These graphs also illustrate that the range of foams characteristics reachable can be further enlarged with the addition of some nanoclays. In fact, when accurate foaming conditions are used, addition of 3 wt% of exfoliated nanoclay leads to a decrease of cell size below 1 μm and to an increase of cell density above 10^{13} cells/cm^3, however, at the expense of foam expansion ratio (~2).

In conclusion, these experimental results show that many parameters can be varied in order to tune the desired foam cellular

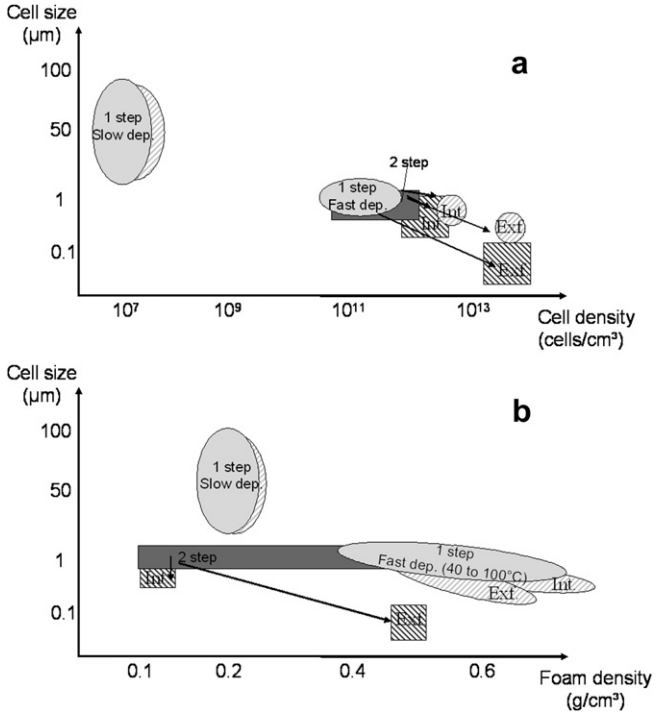

Fig. 16. Schemes representing the cellular morphologies obtained in this work depending on the foaming processes (1 step vs. 2 step) and conditions applied. a) Cell size against cell density, b) cell size against foam density. Striated zones correspond to nanocomposites, « Int » stands for « intercalated nanocomposite » and « Exf » for « exfoliated nanocomposite ».

morphology. In the present work, we focused on selected parameters, such as the foaming process (one-step or two-step), the depressurization rate, the saturation/foaming temperature and the level of nanoclay dispersion, in order to illustrate the high flexibility of this foaming technique. But some other parameters can be varied as well, such as saturation pressure, amount of nanofiller or nanofiller type for example.

4. Conclusion

In this work, foams of neat SAN and SAN/clay nanocomposites have been prepared with two different batch foaming processes with supercritical CO_2 as blowing agent. The amount of CO_2 solubilized in the sample has first been quantified as a function of time with an *ex situ* gravimetric method. An optimal saturation time of 8 h has been estimated from these results to ensure a complete fluid saturation of 1.2 mm-thick samples. We noticed a decrease of CO_2 sorption/desorption rate with the sample based on 3 wt% of exfoliated clay. In contrast, no noticeable effect of the clay on CO_2 solubility has been detected.

The morphology of the foams prepared with the depressurization foaming technique at 100 °C is found to be highly sensitive to depressurization rate, while nanoclay only slightly influences foam density and doubled cell density at best. Decreasing saturation temperature triggers the activation of nanoclay as heterogeneous nucleating agent. In fact, while the clay added only increases slightly cell density of SAN foam at high saturation temperature (>60 °C), its effect is found to be much more pronounced at lower saturation temperature (40 °C), with a jump of the cell density by two orders of magnitude with the exfoliated clay. The effect is less marked for the intercalated nanocomposite. These experiments thus demonstrate the huge influence of foaming conditions when dealing with heterogeneous nucleation. Besides, lower saturation/foaming temperature leads to foams with higher cell density but also with restricted expansion ratio. This drawback has been overcome with the use of the solid-state foaming technique, which allows the preparation of high cell density foams characterized by higher expansion ratios, thanks to the combination of high CO_2 concentration (obtained by saturation at low temperature) and low viscosity (from the high temperature set for foaming).

To conclude, two important teachings can be extracted from this study:

1) Foaming conditions is an important factor which must be taken into consideration when investigating the heterogeneous nucleating efficiency of nanofillers. Indeed, they can affect the final cell density in a very different way despite of identical delamination level.
2) Batch foaming with CO_2 is a very flexible process which gives access to a large range of foams morphologies, going from macrocelullar to microcellular. Submicrocellular foams can even be prepared provided adequate filler and foaming conditions are selected.

Acknowledgements

CERM is grateful for the financial support from the "Interuniversity Attraction Poles" Programme PAI P6/27 – Belgian State – Belgian Science Policy and from the "Région Wallonne" for its financial support in the frame of the WINNOMAT program: PROCOMO. C.D. is "Senior Research Associate" by F.R.S.-FNRS, Belgium. L. Urbanczyk warmly thanks R. Gendron and C.B. Park for their wise comments and fruitful discussion about this work.

References

[1] Jacobs LJM, Kemmere MF, Keurentjes JTF. Green Chem 2008;10:731–8.
[2] Tomasko DL, Burley A, Feng L, Yeh SK, Miyazono K, Nirmal-Kumar S, et al. J Supercrit Fluids 2009;47:493–9.
[3] Ibeh CC, Bubasz MJ. Cell Plast 2008;44:493–515.
[4] Lee LJ, Zeng C, Cao X, Han X, Shen J, Xu G. Compos Sci Technol 2005;65:2344–63.
[5] Lee ST, Park CB, Ramesh NS. Polymeric foams. Florida: Taylor & Francis Group; 2007.
[6] Park CB, Baldwin DF, Suh NP. Polym Eng Sci 1995;35:432–40.
[7] Di Maio E, Mensitieri G, Iannace S, Nicolais L, Li W, Flumerfelt RW. Polym Eng Sci 2005;45:432–41.
[8] Urbanczyk L, Calberg C, Benali S, Bourbigot S, Espuche E, Gouanvé F, et al. Mater Chem 2008;18:4623–30.
[9] Nam PH, Maiti P, Okamoto M, Kotaka T. Polym Eng Sci 2002;42:1907–18.
[10] Taki K, Yanagimoto T, Funami E, Okamoto M, Ohshima M. Polym Eng Sci 2004;44:1004–11.
[11] Mitsunaga M, Ito Y, Okamoto M, Hironaka K. Macromol Mater Eng 2003;288:543–8.
[12] Strauss W, D'Souza NA. J Cell Plast 2004;40:229–41.
[13] Ray SS, Okamoto M. Macromol Mater Eng 2003;288:936–44.
[14] Di Y, Iannace S, Di Maio E, Nicolais LJ. Polym Sci Part B Polym Phys 2005;43:689–98.
[15] Ema Y, Ikeya M, Okamoto M. Polymer 2006;47:5350–9.
[16] Zhai W, Yu Y, Wu L, Ma W, He J. Polymer 2006;47:7580–9.
[17] Shen J, Zeng C, Lee LJ. Polymer 2005;46:5218–24.
[18] Huang HX, Wang JK. Am Soc Mech Eng (ASME) 2005;100:575–80.
[19] Zeng C, Han X, Lee J, Koelling KW, Tomasko DL. Adv Mater 2003;15:1743–7.
[20] Urbanczyk L, Calberg C, Stassin F, Alexandre M, Jérôme R, Jérôme C, et al. Polymer 2008;49:3979–86.
[21] Lee KN, Lee HJ, Kim JH. Polym Int 2000;49:712–8.
[22] Ruckdäschel H, Rausch J, Sandler JKW, Altstädt V, Schmalz H, Müller AHE. Polym Eng Sci 2008;48:2111–25.
[23] Collias DI, Baird DG. Polym Eng Sci 1995;35:1167–76.
[24] Handa YP, Roovers J, Moulinié PJ. Polym Sci Part B Polym Phys 1997;35:2355–62.
[25] Wong B, Zhang Z, Handa PY. J Polym Sci Part B Polym Phys 1998;36:2025–32.
[26] Nawaby AV, Zhang Z. Solubility and diffusivity. In: Gendron R, editor. Thermoplastic foam processing, principles and development. New-Jersey: CRC Press; 2004. p. 1–41.
[27] Pantoula M, Panayiotou CJ. Supercrit Fluids 2006;37:254–62.
[28] Chiou JS, Barlow JW, Paul DR. J Appl Polym Sci 1985;30:2633–42.
[29] Wissinger RG, Paulaitis ME. J Polym Sci Part B Polym Phys 1991;29:631–3.
[30] Zhang Z, Handa PY. J Polym Sci Part B Polym Phys 1998;36:977–82.
[31] Kennedy KA, Roberts GW, Desimone JM. Adv Polym Sci 2005;175:329–46.
[32] Goel SK, Beckman EJ. Polym Eng Sci 1994;34:1137–47.
[33] Arora KA, Lesser AJ, McCarthy TJ. Macromolecules 1998;31:4614–20.
[34] Tsivintzelis I, Angelopoulou AG, Panayiotou C. Polymer 2007;48:5928–39.
[35] Zhai W, Leung SN, Wang L, Kuboki T, Park CB. Proceedings of the blowing agents and foaming processes conference; 2009, Hamburg.
[36] Lee YH, Wang KH, Park CB, Sain MJ. Appl Polym Sci 2007;103:2129–34.
[37] Fujimoto Y, Ray SS, Okamoto M, Ogami A, Yamada K, Ueda K. Macromol Rapid Commun 2003;24:457–61.
[38] Lee YH, Park CB, Wang KH, Lee MH. J Cell Plast 2005;41:487–502.
[39] Gendron R, Champagne MF, Reignier J. Cell Polym 2006;25:199–220.
[40] Zhang P, Wang J, Yang Y, Zhou NJ. Appl Polym Sci 2009;114:1320–8.
[41] Zhu W, Zhou N, Wu H. Polym Eng Sci 2006;46:1728–38.
[42] Youn JR, Park H. Polym Eng Sci 1999;39:457–68.
[43] Han JH, Han CD. Polym Eng Sci 1988;28:1616–27.
[44] Zhang P, Zhou NQ, Wu QF, Wang MY, Peng XF. J Appl Polym Sci 2007;104:4149–59.
[45] Okamoto M, Nam PH, Maiti P, Kotaka T, Nakayama T, Takada M, et al. Nano Lett 2001;1:503–5.